Recent progress in numerical simulations for jet noise computation using LES on fully unstructured meshes

Nicolas Lupoglazoff, Vuillot François

Recent progress in numerical simulations for jet noise computation using LES on fully unstructured meshes

Nicolas Lupoglazoff [1] and François Vuillot [2]
Onera - The French Aerospace Lab, F-92322 Châtillon, France

Numerical simulations of a hot turbulent jet are performed on full unstructured grids with the aim to compute the noise generated in the far field. The jet flow is computed with the Onera CEDRE code using the LES (Large Eddy Simulation) approach and provide the unsteady inputs to the Onera KIM acoustic solver, based on the integral surface FW-H (Ffowcs Williams and Hawkings) approach which is used to reconstruct the acoustic far field. Several unstructured grids of increasing resolution are considered and the results obtained for both the computed jet flow and far field acoustics are compared to measurements carried out in the Onera CEPRA19 anechoic wind tunnel and to previous computations with the same codes but based on structured grids. Results show that unstructured grids allow a better grid tailoring work with an evident ease of construction, compared to the structured grid approach. Very good results are obtained and compare well with available measurements with an unstructured grid of roughly 130 millions cells. These results open the way to the use of unstructured grids in more complex geometries such as those encountered in real life configurations dealing with noise reduction devices or installation effects.

Nomenclature

Cs	=	Constant of the Smagorisky model
D	=	Nozzle exit diameter (m)
f	=	Frequency (Hz)
M	=	Mach number
p	=	Pressure (Pa)
PSD	=	Power spectral density
Re	=	Reynolds number
rms	=	Root mean square value
U	=	Velocity (m/s)
T	=	Temperature (K)
Δ	=	Cell size (m)
γ	=	Ratio of specific heats
Subscripts		
a	=	Ambient conditions
j	=	Jet exit conditions
tot	=	Stagnation conditions

I. Introduction

JET noise contributes largely to the nuisance of aircraft in take-off situations. In order to have the means to control and reduce jet noise, it is desirable to develop reliable and easy to use simulation methods for noise prediction. In that regard, the use of unstructured meshes is seen as an important step to improve on the difficulty to construct structured meshes for real life nozzle geometries and aircraft environment.

This article describes the aeroacoustic computations carried out during 2013 and 2014 on the hot jet issued from Onera Φ80 nozzle at Mach 0.7 with fully unstructured, predominantly tetrahedral meshes. These computations

[1] Research scientist, Fundamental and Applied Energetics department
[2] Research scientist, Fundamental and Applied Energetics department, francois.vuillot@onera.fr

follow many works on the jet noise, e.g. see references[1-15]. More specifically, the present works aim at evaluating the recent versions of the Onera CEDRE code on predominantly tetrahedral meshes on a test case which has been previously computed with the same code on hexahedral and hybrid meshes [9, 14]. The present results will contribute to revisiting the first results obtained on tetrahedral meshes with earlier versions of the CEDRE code, which concluded on the need to insert structured patches into the unstructured mesh[3]. Avoiding the need of structured patches will greatly ease the mesh generation work in complex configurations. The main advantage is that tetrahedral meshes can be easily generated with most grid generation softwares (present grids have been generated with CENTAUR[16]) in any complex geometries.

It has been demonstrated[17] that tetrahedral meshes need some form of gradient limitations to insure stability. Earlier versions of gradient limiters used in CEDRE turned out to be too dissipative to properly capture flow instabilities on tetrahedral grids. The overall methodology was then adapted to include hexahedral zones in the mesh, at least in the vicinity of the jet mixing layers, and it provided satisfactory results[3]. However, for the hybrid grids, the inclusion of the structured zone is disadvantageous in terms of number of stitches (from hexahedra zone to tetrahedra zone), which produce unnecessary small cells, and requires greater sophistication in the construction of the mesh. The other major drawback is that the structured zones cannot produce isotropic grids without strong penalties on the surrounding regions, in terms of number of cells, while in the early jet development region isotropy is desirable. On the contrary this is easily achievable with tetrahedral meshes.

Predicting jet noise was first tested and validated on hexahedral structured meshes, for single and double stream nozzles. The methodology that we are using is the hybrid approach from previous computations at Onera[1-4, 7, 9, 14] which associates a LES unsteady flow solution, using the Smagorinsky subgrid scale model, and an acoustic code for far field reconstruction. The LES solution is computed with the Onera CEDRE code and is stored on particular surfaces surrounding the jet. The stored solution on the surfaces is then fed to the Onera KIM acoustic code, developed by Rahier et al.[11, 12] that relies on several surface integration methods, including the Ffowcs-Williams & Hawkings analogy (FW-H) that is used in the present work.

II. Simulation parameters

A. Jet conditions

In this paper we are considering the Onera PHI80 nozzle, an academic single stream nozzle used for several years to validate numerical simulations[1, 2, 4, 7, 9, 10, 13, 14]. It has a 80mm exit diameter and has been tested in the Onera CEPRA19 anechoic wind tunnel for hot or isothermal conditions. Figure 1 illustrates the nozzle geometry.

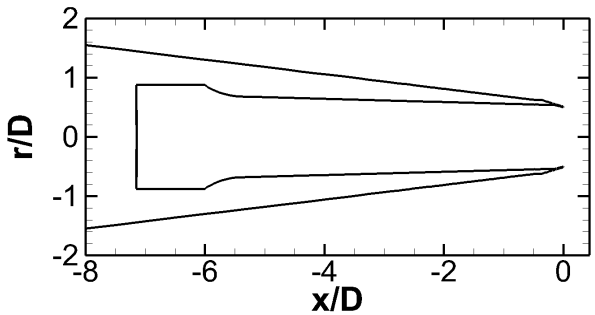

Figure 1. Nozzle geometry

The hot conditions are the one used in the present work and are summarized in table 1.

Table 1. Hot jet characteristics

U_j (m/s)	M_j	T_j/T_a	M_a	T_{tot}/T_a	T_a (K)	Re	p_{tot}/p_a
410	0.7	2.96	1.2	3.2	280	$4.\ 10^5$	1.4

The ambient pressure is set to 101 325 Pa and the nozzle stagnation temperature is 900 K
Finally, the free field velocity is set to Ua = 5 m/s.

B. Numerical settings and boundary conditions

Present LES computations have been carried out with recent versions of Onera in-house CEDRE code (2013 and 2014 versions) relying on second order MUSCL space and one step implicit time schemes. The improved gradient limitation methods available on recent versions were activated. CEDRE is a multi-physics solver which is developed for industrial and research applications in the fields of energetic and propulsion and has been consistently used for jet noise studies.

The resolution of the Navier-Stokes equations is made with a finite volume approach for the conservative variables on generalized unstructured meshes. The simulations were performed following two steps, the first step is performed with higher time steps and is intended to initialize the jet flow across the computational domain, starting from rest conditions. The second step is performed with a reduced time step and is intended to provide unsteady solutions for averaging mean flow, computing flow statistic and perform acoustic computations from solutions stored during this second step. The time steps for the second computational phase are chosen so that, depending on grid resolution, the CFL values is less than 1 in the jet near field and of the order of unity or slightly larger in the vicinity of the nozzle lips and shear layer regions. This second step represents a physical time in excess of 50 ms, that is to say about 250 D/Uj convective time units.

Inside the nozzle, uniform stagnation pressure and temperature profiles are imposed, thus the boundary layers develop freely. Outside the nozzle, static pressure pa = 101 325 Pa is imposed at the outflow conditions. On the lateral and upstream boundaries, static temperature Ta = 280 K and velocity Ua = 5 m/s conditions are imposed. The grid is stretched from a refined zone, in which the jet flow is calculated, to the simulation domain boundaries in order to damp acoustic waves before they reach the borders and thus avoid spurious reflections. The nozzle walls are assumed to be adiabatic.

The computation was performed at the experimental Reynolds number using the Smagorinsky subgrid scale model (Cs = 0.1). Due to the high temperature of the jet flow we decided to rely on thermodynamics properties which are allowed to vary with the temperature.

C. Grid definition

Great care was exercised in defining the unstructured grids used in this work. The idea is to get rid of the structured grid approach or the mixed grid approach which was used in the preceding years and which consisted of imbedding structured patches into an overall unstructured grid. Although the structured grid approaches (either fully structured or mixed structured/unstructured) did work well it implies complex grid construction work that is not well suited to complex configurations as those encountered in practice. Since the recent versions of the code propose advanced gradient limitation procedures it was decided to evaluate them.

Consequently, a consistent unstructured grid hierarchy was constructed. Grids were created with the Centaursoft grid generation tools[16] for a cylindrical computational domain of radius 80D and extending from -29D to 100D in the axial direction (with origin chosen at the nozzle exit plane). These grids are composed of tetrahedra, completed by prisms along nozzle walls. Prisms are intended to produce some degree of mesh anisotropy in the boundary layers, although these are not fully resolved at this stage. The meshes are referenced as 2GG for a coarse version, and 2GM and 3GM for two versions of the medium size meshes. The main properties of these grids are summarized in table 2 below. The 2GG is illustrated on Figure 2.

Table 2. Grid properties

Grid	# Mnodes	# Mcells	# Mfaces	Cell size at nozzle exit	Max cell size at edge of refined zone	Number of cells in azimuthal direction at nozzle exit
2GG	3.1	17.1	34.4	1.0 mm	8.8 mm	251
2GM	11.1	55.5	113.5	0.6 mm	5.5 mm	419
3GM	23.5	130.2	262.3	0.3 mm	4.5 mm	838

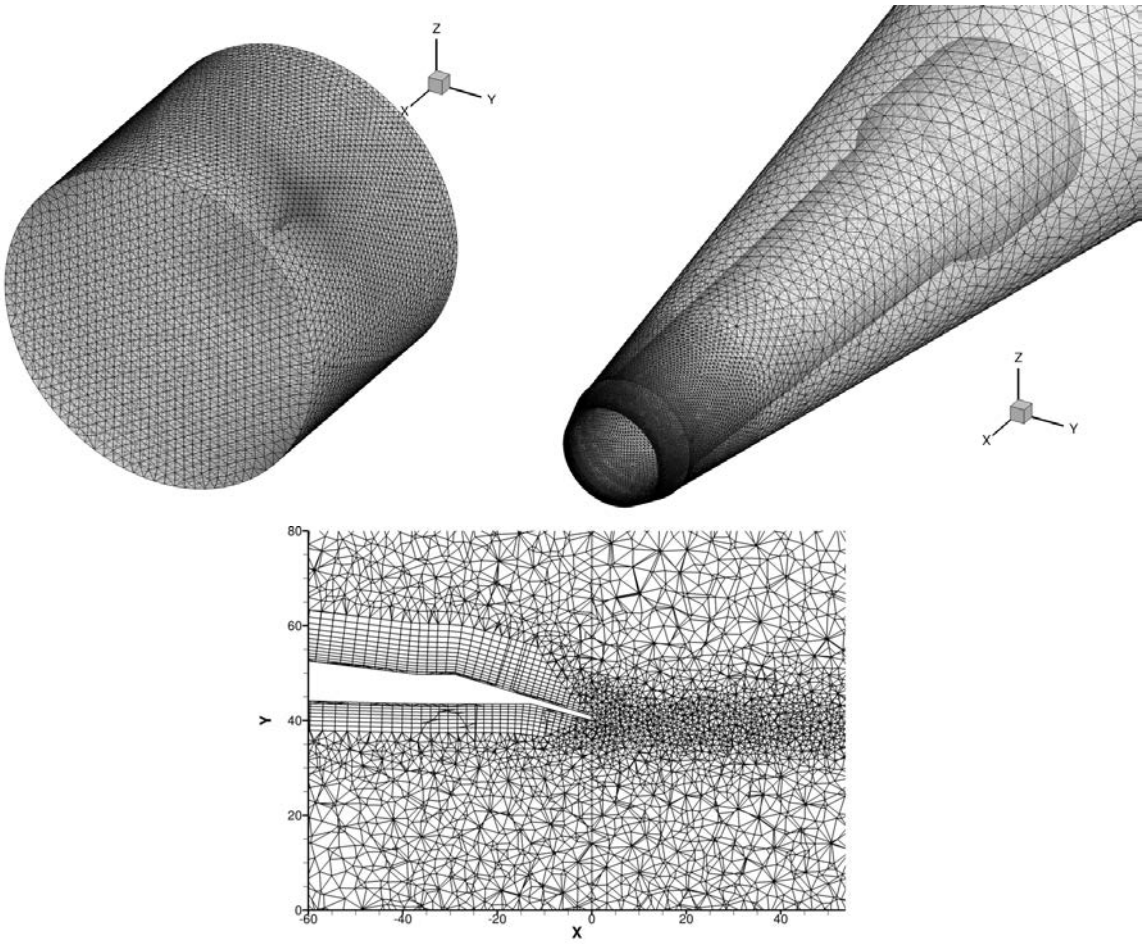

Figure 2. Overview and zoom of the 2GG tetrahedral based mesh.

For these meshes, the refined region is a truncated cone of length 25 D whose radius varies from 2 D (x / D = 0) to 4D (x / D = 25). The largest cell size at the edge of this refined zone leads to an estimated cut-off frequency for the finest 3GM grid in excess of 4000 Hz, based on a 20 point per wave length criterion. A further refinement involves the wake region of the nozzle lip, where the mixing layer develops, and extends over 7.5 D. An additional buffer zone, extending from 25 D to 35 D is used to progressively coarsen the mesh before reaching the computational domain boundaries to avoid spurious wave reflection.

Except for the prismatic zones along the nozzle walls, the tetrahedron grids are mostly isotropic. This is particularly important in regions close to the nozzle exit. Table 2 provides the main characteristics of the grids in terms of spatial resolution. In particular, the grid resolution, Δ, at the nozzle exit can be easily set in the grid generation software and values of Δ/D range from 1.25% for the 2GG grid to 0.375% for the 3GM grid. This results in an azimuthal resolution with cell count ranging from 251 to 838 around the nozzle lip. Recent works[8, 14] have emphasized the importance of providing sufficient azimuthal resolution to properly resolve the early development of the jet shear layer. In this region, the resolution of the 3GM unstructured grid is almost twice as much as the one of the finest structured grids that relied on 480 azimuthal planes.

D. Acoustic far field computations

The far field noise radiation is computed using the Ffowcs Williams & Hawkings[18] (FW-H) porous surface formulation available in the KIM code developed at Onera, see Rahier et al.[12] for more details. This formulation allows to compute time pressure histories at any observer location by integration of the flow fields on a control surface surrounding the jet and containing all the noise sources. It is preferred to the Kirchhoff method that was shown by Rahier et al. to be more exposed to the generation of spurious noise, especially for hot jets. In the present

work, several control surfaces have been used. In particular, as discussed hereafter, the initial surfaces turned out to be too short and were completed by further extensions in the downstream direction. No closure of the surfaces has been used at both extremities to avoid pressure signals contamination by spurious noise generated by the crossing of the surface by turbulent spots. Moreover Rahier et al. showed that the closure does not affect much the results for a sufficiently long surface provided that the turbulence is rather weak on the downstream closing disc. In the present simulation, the far field microphones are located at 75D from the nozzle exit for the directions between 20 deg. and 150 deg., as in the experiments.

III. Flow solution

First the solutions obtained for the three unstructured grids are analyzed in term of jet flow characteristics. In particular, the benefits of a finer grid resolution are clearly illustrated. It must be stressed that for the present computations and contrary to recent works by Lorteau et al.[14], no turbulent triggering is used. The importance of turbulence triggering is still an open question and the present work will give attention to this aspect of the simulations.

A. Jet development

The computed jet development is visible, for the two extreme grids (2GG and 3GM), on figures 3-5. Note that large turbulent scales are less present for the 3GM grid than for the 2GG grid where they result in a faster and more abrupt dispersion of the jet, absent from the 3GM solution. This is especially visible for the axial velocities, figures 3 and 5. As mentioned above, due to the high temperature of the jet flow we decided to rely on variable thermodynamic properties as illustrated on figure 4 which presents the ratio γ of specific heat capacities. On this figure, the effective CFL number is also reported. For the second phase of simulation, the time step is set to 1 μs for the 2GG, 0.5 μs for the 2GM, and 0.3 μs for the 3GM. The CFL values turned out to be less than unity almost everywhere and in the order of unity in the vicinity of the nozzle lips.

The mean and rms axial velocity profiles are shown in figures 6, 7 and compared to experimental measurements of references[4, 5]. The improvement as the grid is refined is clearly visible with 3GM achieving very good comparisons with the measurements. These results also compare well with previous structured computations on the same jet, with the same code[9, 14] . Moreover, the 3GM results are found very comparable to those recently obtained with CEDRE by Lorteau et al. on a refined structured mesh of 240 million cells[14], see figure 11. Both computations produce very good comparisons with available measurements while the 3GM computation presents a clear advantage in term of mesh generation work and in term of CPU cost. For 3GM each job lasted an average of 13 hours CPU on 480 cores on ONERA cluster. It took 12 jobs to pass the transitional first step and 24 jobs for the second step to compute mean field and acoustics. Compared to the reference computation of Lorteau et al. the CPU cost, for computing 1 ms of flow, is found to be reduced by a factor of 3.5, when a second order implicit time scheme is selected.

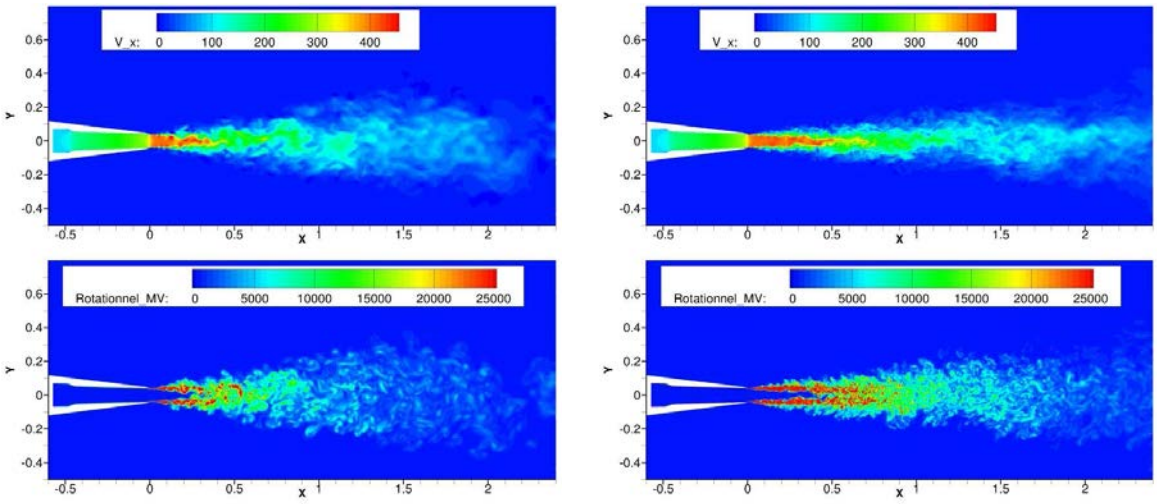

2GG 3GM

Figure 3. Instantaneous fields of axial velocity (top) and vorticity modulus (bottom).

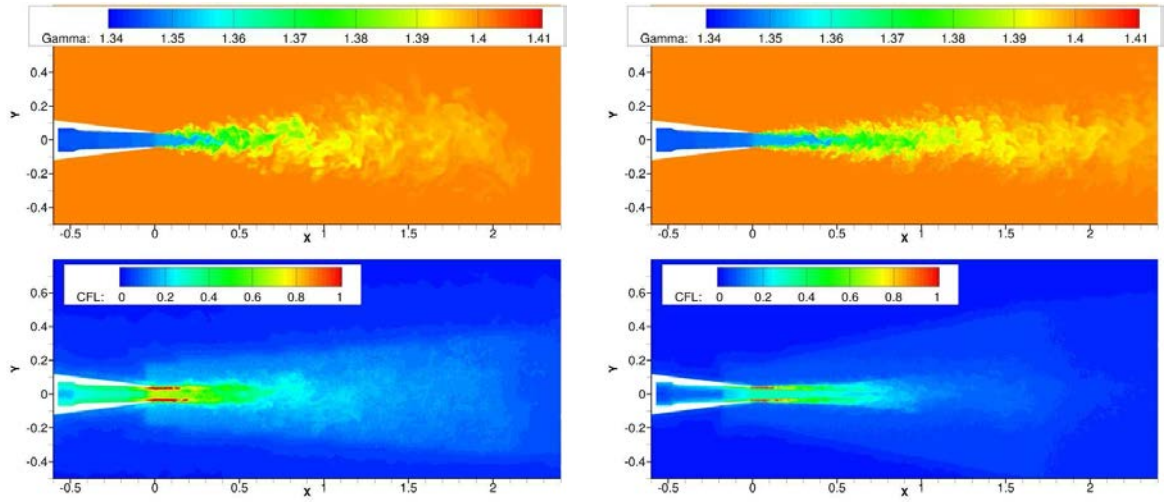

2GG 3GM

Figure 4. Instantaneous fields of ratio specific heat capacities (top) and CFL number (bottom).

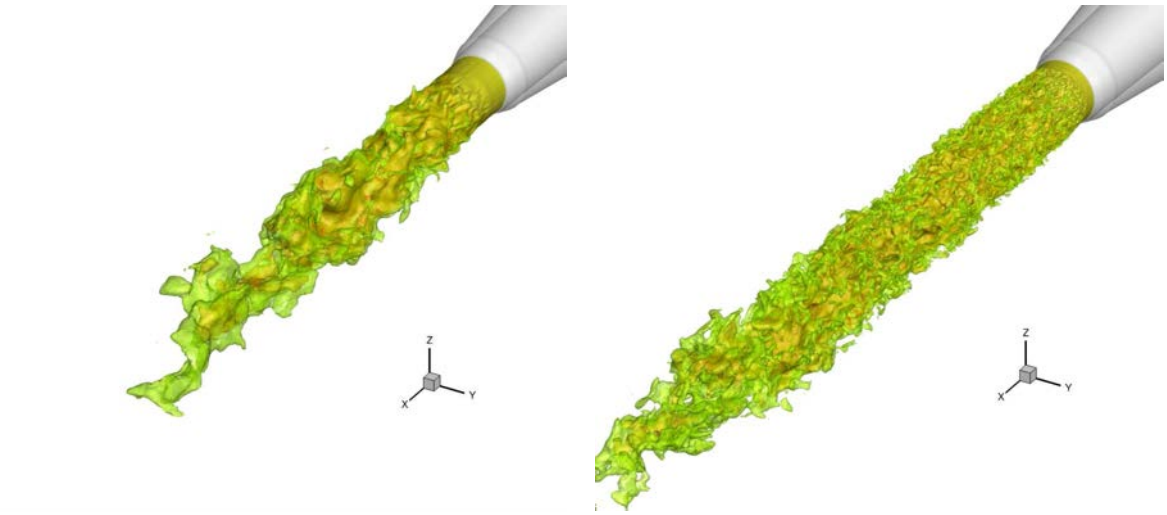

2GG *3GM*

Figure 5. Comparison 2GG / 3GM axial velocity iso surfaces

The present results show a consistent trend both in terms of comparison with previous structured grid results and in term of grid dependency for the present tetrahedral grid family. This permits to validate the use of tetrahedral meshes for jet flow simulations. It is interesting to note that the progressive mesh refinement results in a constant improvement of the results with a very good comparison obtained for the finest mesh, 3GM, compared to available measurements for the jet aerodynamics, with a proper potential core length estimation and turbulence development. Indeed, the potential core length is estimated at Lc = 6.1 D, for both experiment and 3GM computation (with Lc being taken at Ux/Uj = 0.90 on the jet axis). Examining in more details the fluctuation of axial velocity, the finest 3GM mesh leads to a less abrupt turbulence development, which is in good agreement with the measurements (Figure 6).

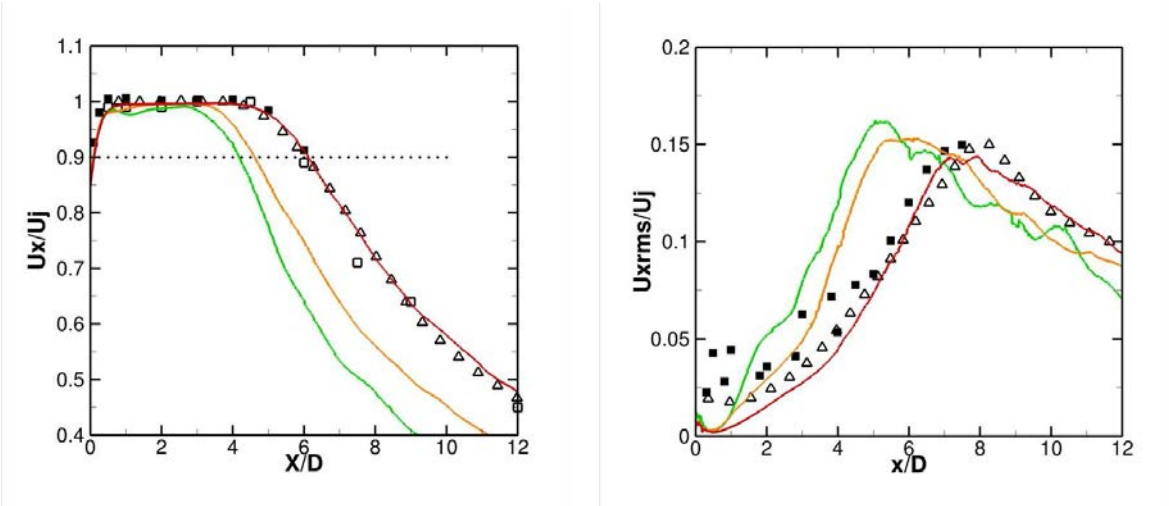

Figure 6. Axial profiles of mean and rms axial velocity.
Green: 2GG, orange: 2GM, red: 3GM – symbols: experiments, square Onera/Φ80, triangles Ahuja et al., [5].

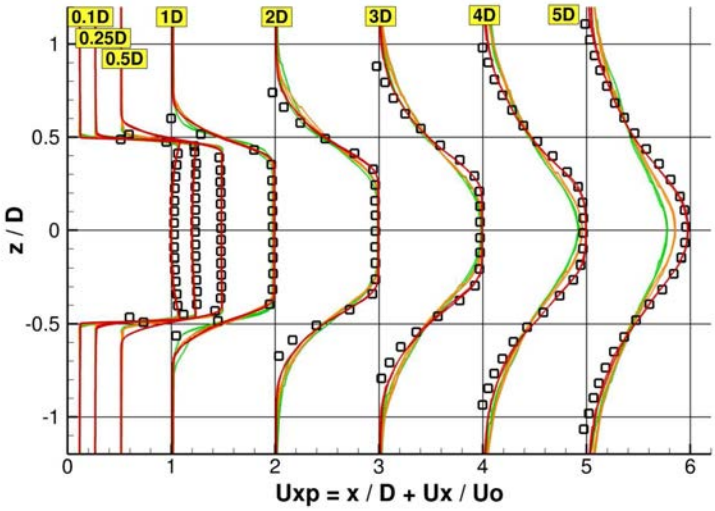

Figure 7. Radial profiles of mean axial velocity.
Green: 2GG, orange: 2GM, red: 3GM – symbol: experiments, Onera/Φ80.

B. Nozzle exit flow

As recent works illustrated the importance of the early flow development, just at the nozzle exit, some attention was given to the computed solution in the nozzle exit region. As mentioned above, no turbulence triggering was used in the present work while Lorteau et al.[14] showed that turbulence triggering is an important aspect for jet flow solution.

Figures 8-10 illustrate the importance of grid resolution on the early flow development just at the nozzle exit. From these figures it is apparent that coarser grids exhibit a retarded transition to turbulence, with large scale vortices which are generated at the nozzle lip, and lead to marked vortex pairing further downstream. On the contrary the finest resolution 3GM grid produces finer structures which are less prone to vortex pairing. As vortex pairing is seen as an additional source of acoustic emission to the far field, the benefit of an increased resolution grid, such as the 3GM grid, is clearly visible. This benefit is clearly apparent on figures 8 and 9, for both the vorticity and pressure fields. When looking at the normalized velocity fluctuations along the nozzle lip line it is clear that finest 3GM grid produces much earlier turbulence development which peaks at 20% at x/D=0.5 and then levels at 16% further downstream (see figure 10) which is in agreement with observed behaviors. Coarser grids 2GG and 2GM exhibit a retarded peak which is at a higher level, close to 20%.

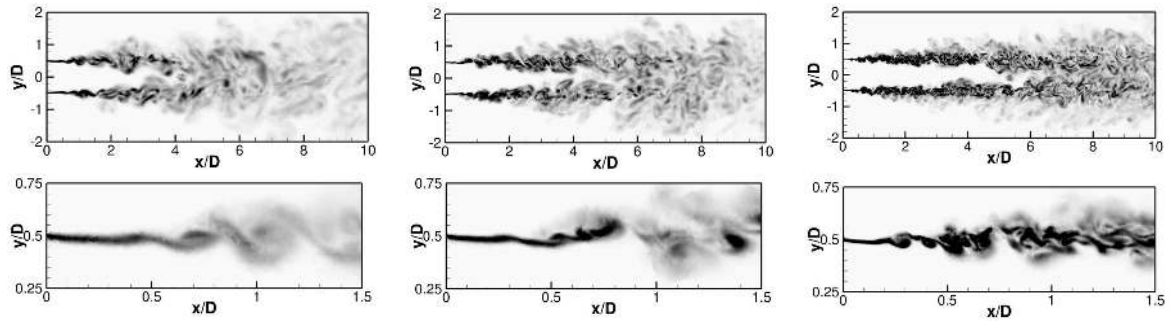

2GG *2GM* *3GM*

Figure 8. Comparison of instantaneous vorticity field in the jet at the nozzle exit

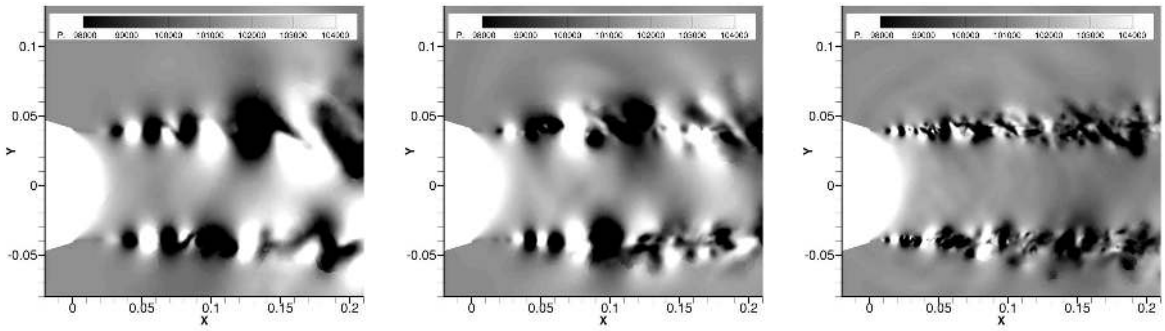

2GG *2GM* *3GM*

Figure 9. Effect of refinement on instantaneous pressure field at nozzle exit.

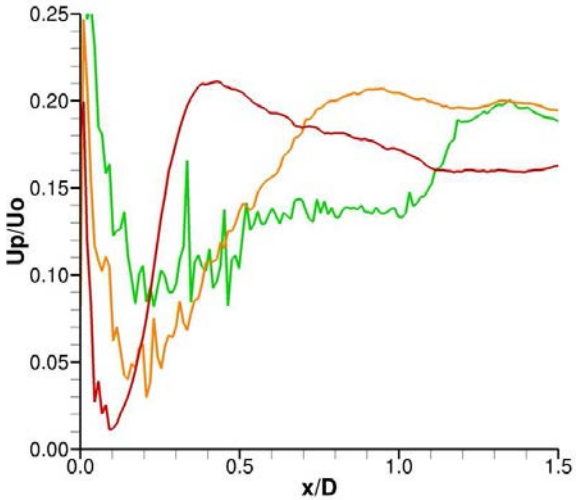

Figure 10. Evolution of normalized axial velocity fluctuations along the nozzle lip line.
Green: 2GG, orange: 2GM, red: 3GM.

Further comparisons were made with the recent computations of Lorteau et al.[14] on a structured grid of 240 million cells with turbulence tripping thanks to a small step inserted inside the nozzle. Figure 11 shows comparisons for the axial profiles of mean and rms axial velocity on the jet axis. This figure shows that very good agreement is obtained between these two computations, performed on very different grids. This demonstrates a satisfactory grid independence of the jet flow solution.

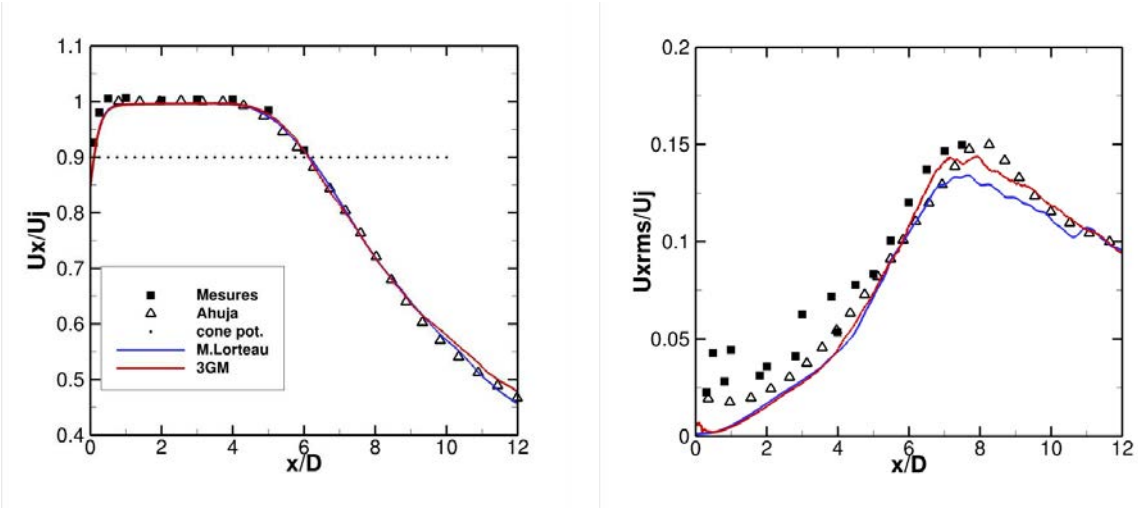

Figure 11. Comparison of the axial evolution on the jet axis of the mean and rms axial velocity for the present 3GM simulation (red line) and Lorteau et al.[14] *Very Fine* computation (blue line) – symbols: experiments, square Onera/Φ80, triangles Ahuja et al.[5].

To go further in this analysis, figure 12 shows the PSD (Power Spectral Densities) of the radial fluctuating velocity recorded at different axial locations along the nozzle lip line. The first plot is obtained from a numerical transducer located inside the nozzle (x/D=-0.25), downstream of the small step used in the work of Lorteau et al.[14]. On that plot the effect of the step, absent from the present computations, is clearly visible as it produces a marked turbulent behavior which is absent from the present 3GM computation. On the next plot at x/D=0.125 one can see that the present 3GM computation is still not fully turbulent with a marked peak at Strouhal number (St = f D/Uj) close to 4, while the triggered computation shows a much broader spectrum. However just downstream of the nozzle, from x/D = 0.25 to x/D = 1.0, the present computation shows broadband spectra in good agreement with the triggered computation, indicating that a correct turbulent transition has occurred, thanks to the fine resolution of the 3GM grid. At this point, the role of turbulence triggering is still an open question and further works are needed to decide whether a refined grid is sufficient to provide the conditions to avoid having to consider turbulence triggering in the nozzle boundary layers.

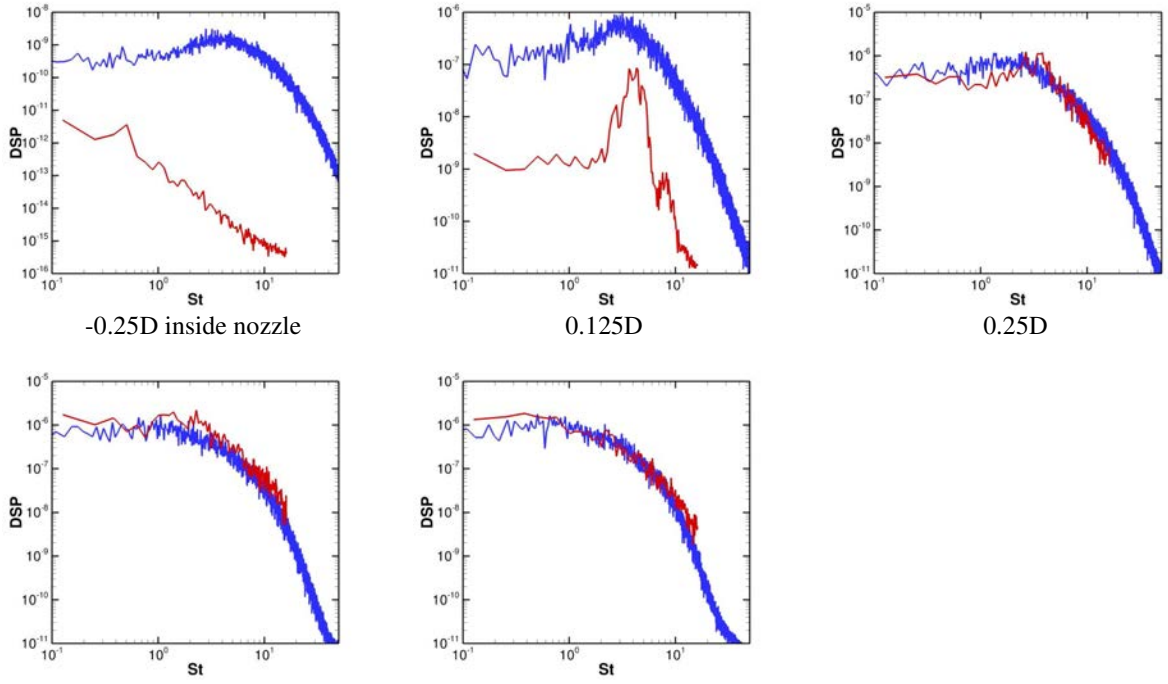

Figure 12. Comparison of PSD of radial fluctuating velocity normalized by Uj at r/D = 0.5 for x/D ∈ {-0.25; 0.125; 0.25; 0.5; 1.0} for the present 3GM computation (red line) and Lorteau et al.[14] *Very Fine* computation (blue line)

In analyzing these results, it is believed that the ability of the code to properly resolve the turbulence at the nozzle outlet is a crucial point for the simulation of the jet and the resulting noise. One of the features that is thought to be important is the proper reproduction of the early transition to turbulence, right at the nozzle outlet. This particular point seems to have a strong dependence on the azimuthal resolution of the grid.

The proper reproduction of this turbulent behavior seems to be essential to capture proper jet development and noise emisssion[15, 14]. In that regard, the refined 3GM grid clearly produces better results, although homogeneous nozzle inlet conditions and no turbulent tripping are yet used at the present stage of these computations. In particular, earlier turbulent transition is visible for the 3GM grid which reduces the formation of the vortex pairing phenomenon. This phenomenon is suspected to be the source of spurious acoustic emissions in less resolved LES computations. In that regard, the high degree of azimuthal resolution permitted by the tetrahedral mesh 3GM (see table 1) is seen as a favorable point to avoid excessive vortex pairing by a better description of isotropic resolved turbulent scales. The importance of azimuthal resolution is discussed by Bogey et al. [8] .

Acoustic far field

A. Integral surfaces

Concerning the far field prediction, several FW-H surfaces were considered, as illustrated on figures 13 and 14. As shown on figure 13, older surfaces were found to be too close to the jet flow and new surfaces were considered, figure 14. However these new surfaces, used for the 3GM computations, appeared to be too short and were later on extended downstream, as illustrated on figure 14. The extension permitted to include low frequency sources, as illustrated on figure 15, that could not be properly taken into account with the shorter ones. To save computational resources the new extended surfaces were evaluated with the coarse grids only and the low frequency correction was simply added to the finer grids, assuming that the coarse grid did properly resolve this low frequency part of the radiated noise.

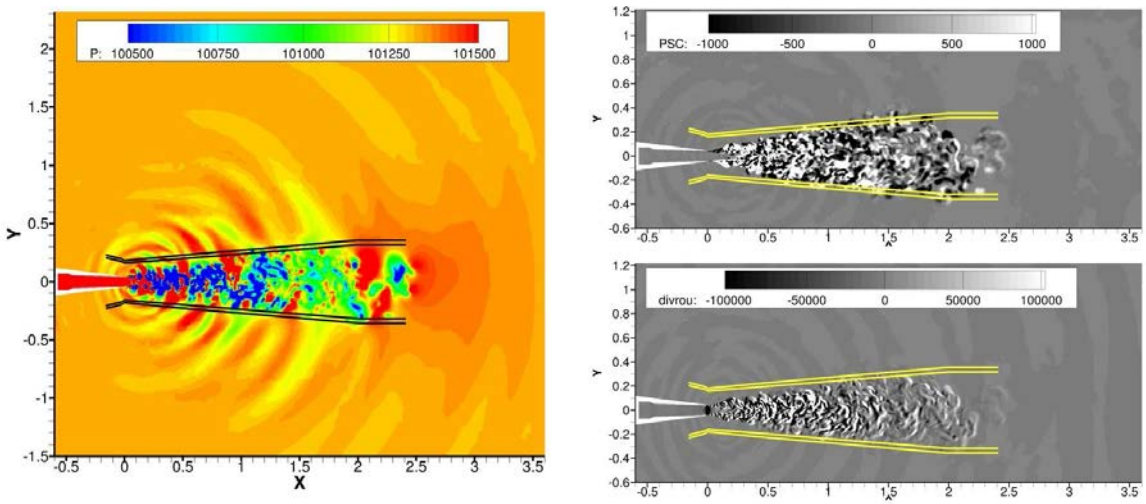

Figure 13. Instantaneous fields of pressure, density gradient and divergence of mass flow, with old storage FW-H surfaces for acoustic KIM code.

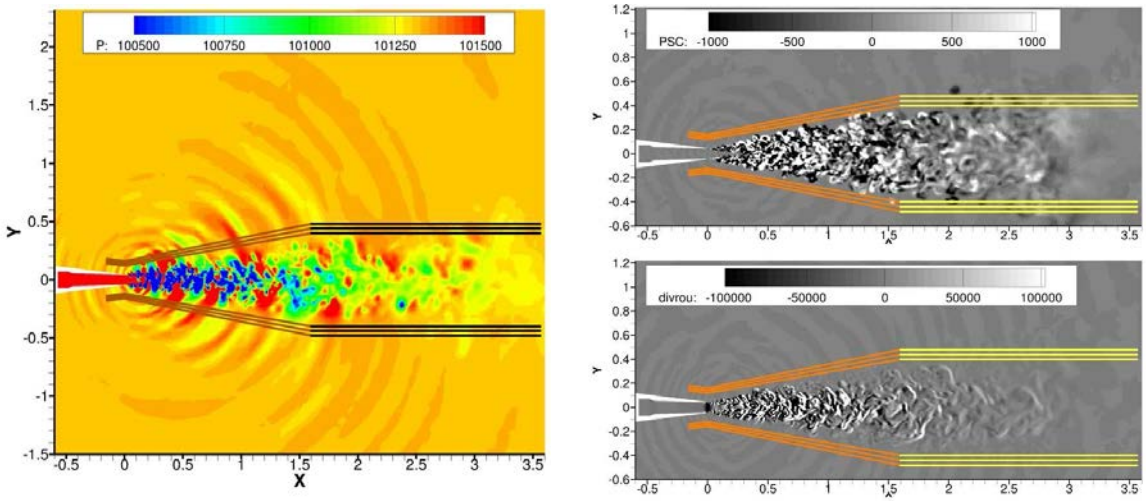

Figure 14. Instantaneous fields of pressure, density gradient and divergence of mass flow, with new storage FW-H surfaces and their downstream extension for acoustic KIM code.

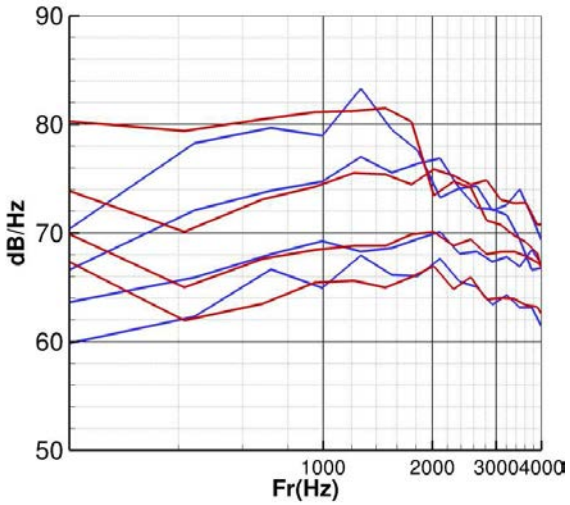

Figure 15. Effect of extended FW-H surfaces on low frequencies (30°, 60°, 90°, 120°) , blue line original surfaces and red line extended surfaces, as computed on the 2GG grid.

B. Far field OASPL

Figure 16 illustrates the far field pressure level (Overall Sound Pressure Level, OASPL) and PSD, reconstructed with the KIM code from LES solution stored on the FW-H surfaces. Levels and spectral contents compare favorably to measurements. It is also apparent on this figure that mesh refinement can significantly improve the prediction of both the spectral contents and the far field levels, with 3GM results being mostly in a ±2 dB band from the measurements. This result is comparable to the far field noise computed by Lorteau et al.[14] on their "*Very Fine*" mesh (structured mesh of 240 million cells). The largest departure is observed in the downstream direction (low angles) and seems to correspond to an underestimation of the low frequency contents. It is anticipated that this discrepancy comes from the initial new FW-H surfaces which miss some low frequency acoustic contributions, although a crude correction was incorporated from coarse grid computation.

We also see the effect of storage in figure 15, which affects only the low frequencies. This helped to correct the low frequencies of the 3GM, but not for 2GM, because the old storage surfaces are different (compare Figure 13 and 14). It is worthwhile to note that the mesh refinement, as expected, extends the cut-off frequency of the computations, as visible on figure 16.

These results, obtained on fully unstructured predominantly tetrahedral meshes, are in line with previous mesh dependency studies obtained, with the same code, on structured meshes, for the same jet, see references[9, 14]. This provides a good confidence in the present computations on tetrahedral meshes.

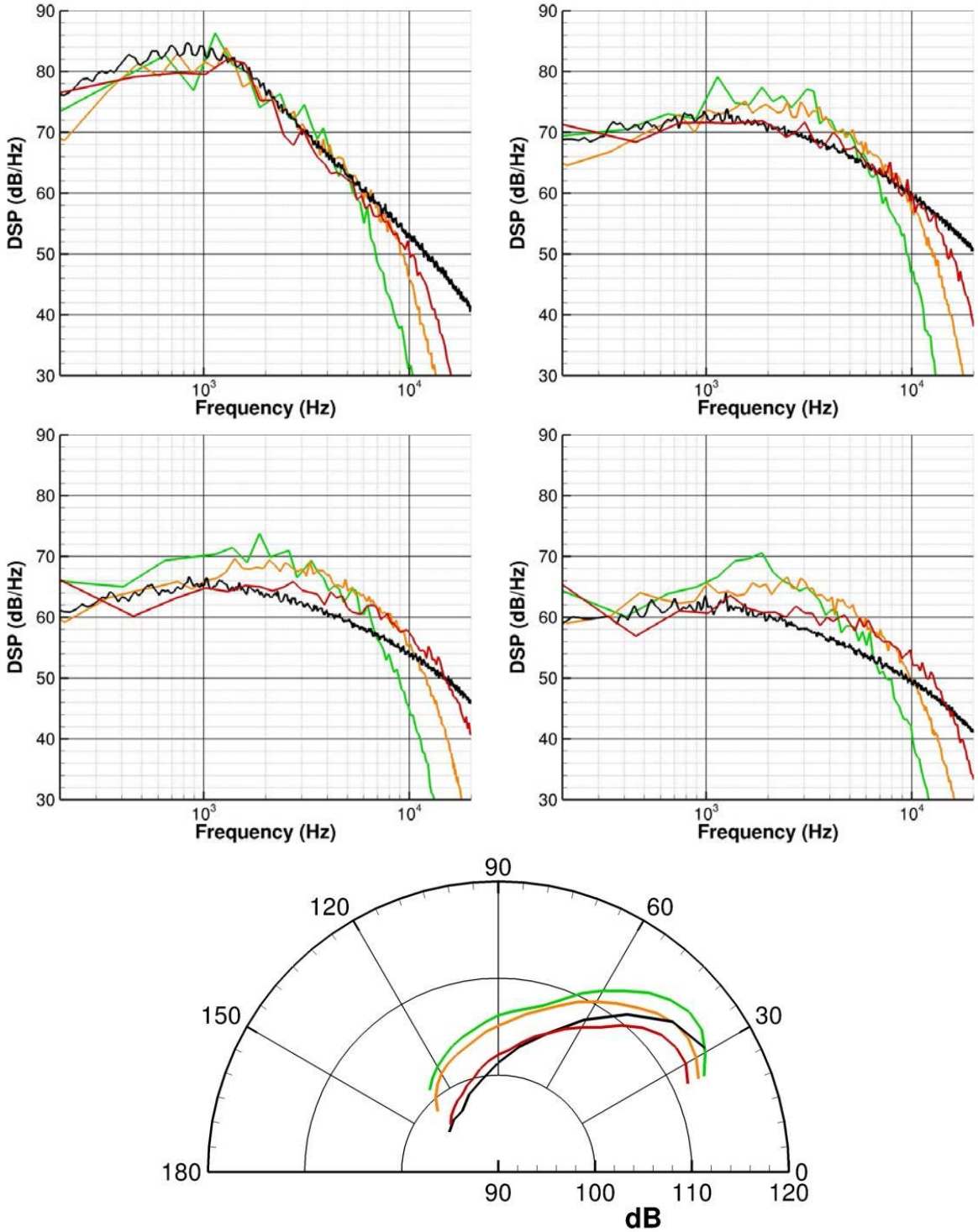

Figure 16. Comparison of average spectra at 30, 60, 90 and 120 degrees, then OASPL.
Green: 2GG, orange: 2GM, red: 3GM - black: experiment, Onera/Φ80 at Cepra19.

IV. Conclusion

The present tetrahedral mesh calculations with coarse and medium grids, with the 2013/2014 versions of the CEDRE code, have provided consistent results, similar to those obtained previously on structured meshes with the same code. For the finest unstructured grid considered in this work, which was composed of 130 millions cells, very good agreement with measurements was presented for both the jet flow solution and the radiated far field noise (levels and spectral contents). This agreement was found comparable to the one obtained from reference structured grid computation on 240 million cells. This provides an essential point of validation to the present numerical approach based on fully unstructured grid for predicting jet noise.

The question of turbulence triggering appears as an open question and further work may be needed to decide if this is a requirement that can be compensated with the higher degree of mesh isotropy and azimuthal resolution permitted by unstructured grids.

The advantage of the full unstructured approach is that coarse (test) grids, which are often sufficient to the overall setting of the computations, can be easily modified to produce more refined grids, in order to provide reliable computations of the solution.

This validation work provides a new opportunity to more freely choose and adapt mesh size, which is promising for applications to more complex geometries where mesh construction is often a limitation. This is particularly crucial for the computations of complex nozzles, including noise reduction devices, such as chevrons, mixers, or of installation effects.

Acknowledgments

The authors want to thanks colleagues from Onera, Mathieu Lorteau, Maxime Huet and Franck Cléro for numerous exchanges and comparisons with their computations of the same jet conditions with the same code on different grids. The presented work has been supported from internal grants from the Fluid Mechanics and Energetics Scientific Branch.

References

[1]Lupoglazoff N., Biancherin A., Vuillot F., Rahier G., "Comprehensive 3D unsteady simulations of subsonic and supersonic hot jet flow-fields. Part 1: aerodynamic analysis," *8th AIAA/CEAS Aeroacoustics Conference,* Paper 2002-2599 (2002).

[2]Biancherin A., Lupoglazoff N., Rahier G., Vuillot F., "Comprehensive 3D unsteady simulations of subsonic and supersonic hot jet flow-fields. Part 2: acoustic analysis," *8th AIAA/CEAS Aeroacoustics Conference,* Paper 2002-2600 (2002).

[3]Lupoglazoff N., Rahier G., Vuillot F., "Application of the CEDRE unstructured flow solver to jet noise computations," *1st EUCASS,* Moscow, 4-7 July, 2005.

[4]Muller F., Vuillot F., Rahier G., Casalis G., Piot E., "Experimental and Numerical Investigation of the Near Field Pressure of a High Subsonic Hot Jet," *12th AIAA/CEAS Aeroacoustics Conference, 8-10 May, 2006, Cambridge, MA, USA,* AIAA-2006-2535.

[5]Ahuja K. K., Lepicovsky J., Tam C. K. W., Morris P. J., Burrin R. H., "Tone-excited jet: theory and experiments," Tech. rep., NASA CR-3538, 1982.

[6]Bridges J., Wernet M. P., "Establishing consensus turbulence statistics for hot subsonic jets," *Proceedings of the 16th AIAA/CEAS Aeroacoustics Conference,* No. AIAA 2010-3751, 2010.

[7]Piot E., Casalis G., Muller F., Bailly C., "Investigation of the PSE approach for subsonic and supersonic hot jets. Detailed comparisons with LES and Linearized Euler Equations results," *Int. J. of Aeroacoustics.*, 5 (2006), pp. 361-393.

[8]Bogey C., Marsden O., Bailly C., "Large-eddy simulation of the flow and acoustic fields of a Reynolds number 10^5 subsonic jet with tripped exit boundary layers," *Physics Of Fluids*, 23 (2011).

[9]Huet M., "Influence of boundary layers resolution on heated, subsonic, high Reynolds number jet flow and noise," *19th AIAA/CEAS Aeroacoustics Conference May 27-29, 2013, Berlin, Germany,* AIAA 2013-2141.

[10]Lorteau M., Cléro F., Vuillot F., "Experimental analysis of the near field pressure of a single stream subsonic jet," *19th AIAA/CEAS Aeroacoustics Conference May 27-29, 2013, Berlin, Germany,* AIAA 2013-2189.

[11]Prieur J., Rahier G., "Aeroacoustic integral methods and efficient numerical implementation," *Aerospace Science and Technology,* 5 (2001), pp. 457-468.

[12]Rahier G., Prieur J., Vuillot F., Lupoglazoff N., Biancherin A., "Investigation of integral surface formulations for acoustic post-processing of unsteady aerodynamic jet simulations," *Aerospace Science and Technology,* 8 (2004), pp. 453-467.

[13]Labbé O., Peyret C., Rahier G., Huet M., "A CFD/CAA coupling method applied to jet noise prediction," *Computers and Fluids,* 86 (2013), pp. 1-13

[14]Lorteau M., Cléro F., Vuillot F., "Recent progress in LES computation for aeroacoustics of turbulent hot jet. Comparison to experiments and near field analysis," *20th AIAA/CEAS Aeroacoustics Conference,* AIAA paper, 2014-3057.

[15]Bogey C., Marsden O., Bailly C., "Influence of initial turbulence level on the flow and sound fields of a subsonic jet at a diameter-based Reynolds number of 10^5," *Journal of Fluid Mechanics,* 701 (2012), pp. 352-385.

[16]Centaur grid generation software: *https://www.centaursoft.com*

[17]Haider F., Croisille J.-P., Courbet B., "Stability of the cell centered finite-volume MUSCL method on unstructured grids," *Numerische Mathematik;* 113 (2009), pp. 555-600 ; Springer Verlag.

[18]Ffowcs Williams, J. E. and Hawkings, D. L., "Sound generation by turbulence and surfaces in arbitrary motion," *Philosophical Transactions of the Royal Society of London A*, 264 (1969), pp. 321-342.